

Numerical analysis of ammonia homogenization for selective catalytic reduction application

Jakov Baleta^{a*}, Matija Martinjak^b, Milan Vujanović^a, Klaus Pachler^c, Jin Wang^d, Neven Duić^a

^aFaculty of Mechanical Engineering and Naval Architecture

University of Zagreb,

Ivana Lučića 5, 10 002 Zagreb, Croatia

e-mail: jakov.baleta@fsb.hr, milan.vujanovic@fsb.hr, neven.duic@fsb.hr

^bTE-TO Sisak, HEP Proizvodnja d.o.o.

Industrijska cesta 10, 44010 Sisak, Croatia

e-mail: matija.martinjak@gmail.com

^cAVL List GmbH,

Alte Poststraße 152, 8020 Graz, Austria

e-mail: klaus.pachler@avl.com

^dSchool of Energy and Environmental Engineering

Hebei University of Technology,

Xiping Road No.5340, Beichen District, Tianjin, 300401,China

e-mail: wjwcn00@163.com

* Corresponding author

ABSTRACT

Selective catalytic reduction based on urea water solution as ammonia precursor is a promising method for the NO_x abatement from exhaust gases of mobile diesel engine units. It consists of injecting the urea-water solution in the hot flue gas stream and reaction of its products with the NO_x over the catalyst surface. During this process flue gas enthalpy is used for the urea-water droplet heating and for the evaporation of water content. After water evaporates, thermolysis of urea occurs, during which ammonia, a known NO_x reductant, and isocyanic acid are generated. The uniformity of the ammonia before the catalyst as well as ammonia slip to the environment are important counteracting design requirements, optimization of which is crucial for development of efficient deNO_x systems.

The aim of this paper is to show capabilities of the developed mathematical framework implemented in the commercial CFD code AVL FIRE[®], to simulate physical processes of all relevant phenomena occurring during the SCR process including chemical reactions taking part in the catalyst. First, mathematical models for description of SCR process are presented and afterwards, models are used on the 3D geometry of a real SCR reactor in order to predict ammonia generation, NO_x reduction and resulting ammonia slip. Influence of the injection direction and droplet sizes was also investigated on the same geometry. The performed study indicates importance of droplet sizes on the SCR process and shows that counterflow injection is beneficial, especially in terms of minimizing harmful ammonia slip to environment.

Key words: computational fluid dynamics, NO_x reduction, selective catalytic reduction, spray preparation, urea-water solution, ammonia slip

1. INTRODUCTION

Despite almost quarter century of global efforts on the reduction of harmful atmospheric emissions, the latest reports on anthropogenic global warming indicate that still increased and joint global action is necessary in order to reduce greenhouse gas emission and harmful emissions in generally (“Cause of climate change,” n.d.). Among harmful emissions nitrogen oxides, referred commonly as NO_x , take important place. Although European Environment Agency (EEA)-33 emissions of nitrogen oxides (NO_x) from transport decreased by 39% between 1990 and 2014 (European Environment Agency, n.d.), they are still subject to ever increasing emission standards (*European Union, Regulation (EC) No 715/2007, 2007*) in order to minimize their harmful environmental impact. In 2014, the most significant sources of NO_x emissions were road transport (40.15 %), energy production and distribution (21.33%) and the commercial, institutional and household (13.38%) sectors (EEA, 2014).

Methods of NO_x control may be categorized according to the stage of combustion they tackle into pre-combustion, combustion and post-combustion methods (Tayyeb Javed et al., 2007). Selection of individual method or combination of methods is always conditioned by economic balances and legislation. Pre-combustion methods imply fuel treatment in order to decrease amount of fuel bounded nitrogen, which is fairly expensive and thus not applicable for real industrial cases. Lately, there was increasing trend of replacing fossil fuels with alternative fuels (Honus et al., 2016) to some extent, thereby co-firing the mixture of fossil and alternative fuel (Mikulčić et al., 2016). Moreover, related to combustion NO_x control methods, first option consists of regulation of the excess air, keeping at the same time in mind the fact that it directly affects unburned carbon emissions. Combustion air staging creates fuel-rich primary zone and fuel-lean secondary zone, suppressing that way creation of fuel NO_x . Similarly like combustion air, fuel can also be staggered through creating a fuel-rich secondary combustion zone, where NO_x formed in the primary combustion zone is decomposed. Exhaust gas recirculation, a

technique frequently employed in modern internal combustion engines (Kozarac et al., 2014), as well represents one of the primary NO_x reduction measures which can significantly reduce thermal NO_x generation by lowering combustion temperatures and excess air. Porous burners have characteristics that make them suitable for NO_x reburning and their usage has been growing in extent lately (Mujeebu et al., 2009).

Recent tightened EURO 6 NO_x emission standard introduced significant reduction of NO_x emissions to 80 mg/km compared against 180 mg/km defined in previous EURO 5 standard (Grout et al., 2013). This requirement cannot be met using described primary NO_x reduction techniques anymore and solution should be found in utilizing exhaust gas aftertreatment techniques. During the last decade urea water solution (UWS) based selective catalytic reduction (SCR) broke through as a most promising deNO_x method for transportation sector (Baleta, 2013). Since its inception in the early 1970s in stationary industrial applications (Fang and DaCosta, 2003), UWS-SCR has grown in extent covering also mobile applications of road vehicles and marine transport.

UWS is precursor for ammonia generation due to its toxicity and harmful environmental impact. Usually a 32.5%w urea solution, commercially named AdBlue, is sprayed into hot exhaust gases where few processes are taking part sequentially. First, the water evaporates from the droplets. Then, ammonia is generated through thermal decomposition of urea and hydrolysis of isocyanic acid if the temperature of the exhaust gases is suitably high. The resulting ammonia is dispersed due to interaction with turbulent fluctuations within gas flow. So, the task of UWS-SCR system before the catalyst is to provide suitable residence time for complete thermal decomposition and to ensure ammonia uniformity before the catalyst. Otherwise, many problems can occur – from deposit formation and passivation of the catalyst parts to the toxic ammonia slip in environment. Additional design challenges to the equipment manufacturers are transient working conditions of

internal combustion engines for mobile applications and confined engine space, which makes design of the SCR system and spray preparation task far more than trivial.

Presented literature overview is combination of recent experimental and numerical efforts in order to better understand physical and chemical phenomena taking place in UWS-SCR system and to provide optimal design guidelines. (Jeong et al., 2008) numerically investigated effects on injector location, configuration and operating conditions on local uniformity of NH_3 before the catalyst. (Liao et al., 2015) experimentally analysed spray characteristics of four commercially available injectors by employing non-intrusive measuring techniques with the aim of assessing the spray quality in different flow conditions. (Lee et al., 2012) experimentally studied two types of mixing chambers design effect on urea thermal decomposition. Experimental work carried in (Grout et al., 2013) showed that UWS spray evaporation is an important step that could also entail usage of additional evaporation strategy such as static mixer, especially in confined space of engine. (Cho et al., 2014) performed numerical analysis of UWS-SCR system by varying three different lengths of decomposition pipe and by employing two different types of static mixers. (Oh and Lee, 2014) experimentally examined basic spray characteristics of urea injector. They determined optimal location and mixer type in the flow conditions closely resembling those in real exhaust systems of road vehicles diesel engines. (Tian et al., 2015) numerically investigated the distance between UWS nozzle and reactor from the perspective of UWS droplet evaporation and urea decomposition. Numerical simulation of marine SCR system under engine like operating conditions was conducted by (Choi et al., 2015). Different combinations of mixing chamber and swirl type static mixer were investigated with respect to ammonia homogenization. Also, (Chen and Lv, 2015) were dealing with design of compact integrated SCR and exhaust muffler unit for marine diesel applications. Numerical simulations were performed with respect to unit pressure loss and NO_x conversion efficiency. (Varna et al., 2015) conducted experimental and numerical assessment of UWS droplets impingement and mixing

but they also analysed only processes upstream of the catalyst with respect to ammonia preparation. (Smith et al., 2014) studied deposit formation in urea SCR system both experimentally and numerically. They developed predictive subroutine for deposit occurrence based on thorough parametric analysis. (Betageri et al., 2016) investigated effect of injection configurations on the deposit formation in the SCR system of a diesel engine by combination of vehicular trials and detailed CFD simulation. Work carried out by (Sadashiva Prabhu et al., 2017) took into account deposit formation in SCR pipe for different flow rates in the low temperature range between 150 and 250°C. However, the deposition formation model was not developed, but solely the remaining wall film after water evaporation was assumed to become deposit. From the standpoint of reductant dosing control, special challenge lies in managing the SCR system in a way that will enable high denitrification efficiency together with low ammonia slip. (Zhang and Wang, 2016) investigated the adaptive sliding-mode observer design problem for the selective catalytic reduction (SCR) system in diesel-engine aftertreatment system as a support for dosing system. Optimal dosing and sizing strategy of two-cell SCR system was proposed in the work of (Zhang et al., 2016) on the basis of dynamic programming algorithm.

It can be seen that most of the research from the available literature deals with processes happening upstream of the catalyst. Studies taking into account the complete SCR system including dosage, mixing chamber and catalyst are not so frequently encountered. Therefore, the aim of this work is the numerical analysis of ammonia homogenization in the geometry of real SCR system. This research represents continuation of the research conducted previously where validated numerical framework was established for SCR and SNCR applications (Baleta et al., 2016). This manuscript is composed as follows. In the proceeding part, relevant mathematical models composing numerical framework for UWS-SCR are described. Afterwards, a 3D turbulent reacting flow CFD model involving reaction mechanism on the catalyst surface is applied on the real SCR system geometry with exhaust gas composition, flow rate and

temperature resembling those of diesel engines. Six simulated cases are divided into two simulation groups in order to study the influence of injection direction and droplet size on ammonia generation and uniformity. Finally, important findings are summarized together with recommendations for future research work.

2. MATHEMATICAL MODEL

In order to accurately represent all relevant physical phenomena occurring during the injection of urea-water solution (UWS) into hot flue gases mathematical description of processes is needed as follows:

- solution of gas phase;
- description of spray droplets motion inside the domain;
- evaporation of urea-water solution droplets;
- thermal decomposition of urea;
- chemical reactions taking place on the catalyst surface;
- accurate and computationally economical representation of turbulence.

2.1. Gas phase

Mass conservation law (continuity equation) for differential element of fluid in Cartesian coordinate system can be expressed as follows:

$$\frac{\partial \rho}{\partial t} + \frac{\partial}{\partial x_j} (\rho u_j) = 0 \quad (1)$$

where ρ is fluid density, t represents time, x_j Cartesian coordinates and u_j velocity vector components. For incompressible fluid, equation (1) states that the divergence of velocity is equal to zero.

Momentum conservation law for infinitesimal, incompressible Newtonian fluid element can be stated as:

$$\frac{\partial}{\partial t}(\rho u_i) + \frac{\partial}{\partial x_j}(\rho u_i u_j) = -\frac{\partial p}{\partial x_i} + \mu \frac{\partial^2 u_i}{\partial x_j \partial x_j} + \rho f_i \quad (2)$$

Momentum conservation law equations for Newtonian fluid together with continuity equation (1) are also called Navier-Stokes equations according to the researchers who were first to derive them.

Energy conservation law can be written as:

$$\frac{\partial}{\partial t}(\rho i) + \frac{\partial}{\partial x_j}(\rho i u_j) = -p \frac{\partial u_j}{\partial x_j} + \frac{\partial}{\partial x_j}(\lambda \frac{\partial T}{\partial x_j}) + \rho f_i v_i + \frac{\partial(\tau_{ji} v_i)}{\partial x_j} \quad (3)$$

where i is specific internal energy of fluid.

Significant commonalities between presented governing equations justify introduction of a general variable φ , which enables us to write general conservative form of all fluid flow equations as follows:

$$\frac{\partial}{\partial t}(\rho \varphi) + \frac{\partial}{\partial x_j}(\rho \varphi u_j) = \frac{\partial}{\partial x_j}(\Gamma_\varphi \frac{\partial \varphi}{\partial x_j}) + S_\varphi \quad (4)$$

General transport equation of scalar quantity could be decomposed on characteristic members, each having distinguished physical meaning and inherent properties. First term on the left hand side of the equation (4) represents time rate of change of general variable φ , second term on the same side is convective transport of the same variable, first term on the right hand side describes diffusional transport of φ , whilst the last term of the equation represents source/sink of the variable φ due to various mechanisms, not being covered by the three previous ones. General transport equation (4) represents basic equation upon which the numerical theory of CFD is being built.

2.2. UWS spray

The most commonly used method for spray calculation today is Discrete Droplet Method (DDM) (Yuen and Chen, 1976), although Euler Eulerian size of class model has drawn attention

recently for specific tasks, such as computation of spray in the vicinity of nozzle (Petranović et al., 2017). Taking into account current state of CFD techniques, it would be impossible to solve differential equations for the trajectory, momentum, heat and mass transfer of every single spray droplet. DDM simplifies spray modelling by introducing parcels which are groups of droplets with the same size and physical properties. That way, only differential equations of parcels are numerically solved which significantly reduces computation time and required computing power.

Droplet parcels are introduced in the flow domain with initial conditions of position, size, velocity, temperature and number of particles inside the parcel. Lagrangian description of motion is then used for tracking the parcels through the computational grid.

From the Newton's second law of motion, which states that the net force on an object is equal to the rate of change of its linear momentum in an inertial reference frame, follows droplet momentum equation:

$$m_d \frac{du_{id}}{dt} = F_{idr} + F_{ig} + F_{ip} + F_{ib} \quad (5)$$

where m_d and u_{id} are droplet mass and droplet velocity respectively, F_{idr} is the drag force, F_{ig} is a force including the effects of gravity and buoyancy, F_{ip} is the pressure force and F_{ib} summarizes other external forces. Comparing the magnitude of all forces (Ström et al., 2009), the drag force and gravity effects are only relevant for UWS spray injection application. Therefore follows:

$$m_d \frac{du_{id}}{dt} = F_{idr} + F_{ig} \quad (6)$$

After integrating above equation, u_{id} could be obtained, and from this we can solve differential equation for the trajectory:

$$\frac{dx_{id}}{dt} = u_{id} \quad (7)$$

In commercial CFD code AVL FIRE[®] turbulent dispersion, evaporation of droplets, the droplet-

gas momentum exchange, secondary break-up, droplet collision and droplet-wall interaction are covered with set of models that are summarized in (AVL, 2013).

Droplet evaporation can be described by different methods in the rising level of complexity, such as: constant droplet temperature model, infinite diffusion model, effective diffusion model, vortex model and Navier-Stokes solution. For the purpose of this research Abramzon/Sirignano evaporation model was used to perform calculations (Abramzon and Sirignano, 1989). This model represents the extension of classical droplet vaporization model (Dukowicz, 1979) and includes important effects such as variable physical properties, non-unitary Lewis number in the gas phase and influence of Stefan flow on the heat and mass transfer. It requires a relatively small amount of computational time per droplet and therefore is convenient for spray calculations. Despite numerous experimental studies (Musa, S. N. A., Saito, M., Furuhashi, T., Arai, 2006; S. Kontin, A. Höfler, R. Koch, 2010; Wang et al., 2009) theoretical understanding of evaporation and decomposition of UWS droplets is still far from satisfactory. Theoretical study conducted by Birkhold et al. (Birkhold et al., 2007) is implemented in AVL FIRE[®] and represents optimum between results accuracy and computational demands. At elevated temperatures the evaporation of liquid starts. Since water has a boiling point below starting temperature of urea thermolysis, the gaseous species first consist mainly of water. Whether urea vapour also produced is questionable, since urea is known to decompose directly via thermolysis from solid or liquid. Birkhold's approach assumes two stage process – pure water evaporation until the droplet is composed of urea only and subsequent thermolysis. It is assumed that droplets remain spherical throughout the evaporation and decomposition processes, as well as that no crystallization of urea occurs.

In order to evaluate the influence of dissolved urea on the evaporation of water, Rapid Mixing model is employed. Within this model infinite high transport coefficients are assumed for the liquid phase, resulting in spatial uniform temperature, concentration and fluid properties in the

droplet, but those quantities will change in time (Abramzon and Sirignano, 1989). It has been confirmed as satisfactory for UWS spray applications by several authors (Abu-Ramadan et al., 2011; Birkhold et al., 2007). The variation of urea concentration of the droplet can be evaluated by:

$$\frac{dY_u}{dt} = -\frac{\dot{m}_{vap}}{m_d} Y_u \quad (8)$$

It should be noted that mass flow from liquid to gaseous phase is defined to be negative.

Urea melts at 406 K and the thermal decomposition of urea into ammonia and isocyanic acid starts. It is generally accepted that two different ways for the thermal decomposition can be assumed:

- evaporation of molten/solid urea to gaseous urea, which decomposes in gas phase into NH_3 and HNCO ;
- direct thermolysis from molten/solid urea to gaseous NH_3 and HNCO .

This model assumes the latter option and since there is no phase change of urea, an alternative way as used for the evaporation of water must be taken to calculate the urea decomposition rate.

For this purpose Arrhenius-type expression is used:

$$\frac{dm_u}{dt} = -\pi D_d A e^{(-E_a/RT_d)} \quad (9)$$

where A is a frequency rate and E_a is activation energy. Experimental data from Yim et al. (Yim et al., 2004) were used for a default parameter fit.

The most favoured method for modelling turbulent flows in industrial applications is the Reynolds Averaged Navier Stokes equations (RANS) with an appropriate turbulence model. Many turbulent models employ the concept of a turbulent viscosity or a turbulent diffusivity to approximate the turbulent Reynolds stresses and the turbulent heat fluxes. Turbulence was modelled by the advanced k- ζ -f model which was proved more suitable for strong swirling

flows such as those that can be found in internal combustion engines applications (Hanjalić et al., 2004).

2.3. Selective catalytic reduction

Once urea-water-solution spray is injected into hot exhaust gas stream before SCR catalyst, water content evaporates from UWS. Afterwards, ammonia is generated through thermal decomposition of urea and hydrolysis of isocyanic acid (Birkhold et al., 2007):



Hydrolysis of isocyanic acid:

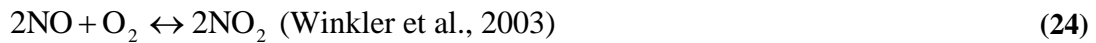


Generated ammonia takes part in various deNO_x reactions as a reductant (Fang and DaCosta, 2003):



The reaction model employed in this work is developed for the simulation of HSO (Hydrolysis-SCR-Oxidation) catalysts. This type of NO_x reduction system consists of three different coating sections where following processes are taking place: the hydrolysis of isocyanic acid, the selective catalytic reduction of NO_x with ammonia and the oxidation of ammonia. The model explicitly takes into account the ad/desorption of ammonia at the solid surface and therefore is able to resolve transient operating conditions (AVL, 2013). This model is based on the work carried by (Winkler et al., 2003; Wurzenberger and Wanker, 2005). The following reactions are taken into account:





It can be seen that catalyst is divided into three functional parts, depending upon which reactions are taking place, namely hydrolysis part, deNOx part and oxidation part. More details about reaction constants can be found in (Winkler et al., 2003; Wurzenberger and Wanker, 2005).

3. NUMERICAL SIMULATION SETTINGS

Figure 1. depicts the computational domain used in this research together with the boundary surfaces. Simulation is performed by injecting UWS inside the given geometry having length of 1.53 m. After grid dependency investigation domain consisting of 84 672 control volumes was selected for parametric study.

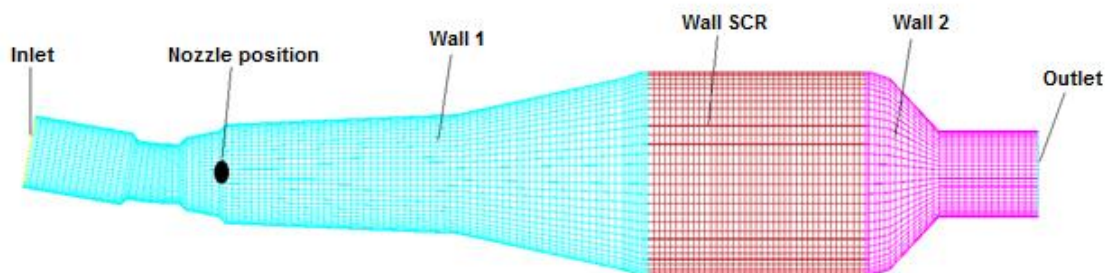


Figure 1. Discretized geometry of the SCR system

Figure 1. also indicates nozzle position, which is located at the beginning of conically shaped mixing chamber. Spray cone angle was 60°. Table 1. shows variation of time step size during

simulation progress. It can be seen that during the nozzle opening time from 0.1 to 0.4 s the time step is refined in order to capture transient phenomena of UWS droplets evaporation and thermal decomposition.

Table 1. Variation of time step size for simulation

Time step			Δt
	up to	0.1 s	0.005 s
	up to	0.4 s	0.002 s
	up to	0.8 s	0.005 s
End time	0.8 s		

At the inlet a mixture of gases represented by Table 2. with the temperature of 400 °C and a mass flow rate of 850 kg/h enters the domain. The simulated mixture of gases approximates the real exhaust gas composition of diesel road vehicles. Turbulence on the inlet is described with turbulent kinetic energy of 0.001 m²/s² and turbulent length scale of 0.00304 m.

Table 2. Exhaust gas composition on the inlet

Chemical species:	Mass fraction:
NO	6.7553e-04
NO ₂	5.1709e-04
NH ₃	1.0e-10
H ₂ O	7.7e-02
O ₂	1.3e-01
CO ₂	9.0e-02
HCNO	1.0e-10
N ₂	0.701807







Regarding the catalyst, following settings were used: density of the active site is 1700 kg/m³, thermal conductivity is 0.4 W/(m·K) and specific heat capacity is 1200 J/(kg·K). The initial temperature of the monolith is 400°C with cell density of 400 1/ in². Pressure drop was calculated by employing „Tube friction“ model (AVL, 2013). In order to save calculation

resources, calculation was initialized with catalyst substrate completely loaded with ammonia. Thus, it was possible to draw conclusion after simulating only one injection cycle.

At the outlet of the domain, the pressure boundary condition with 100 000 Pa was applied, whilst catalyst wall heat transfer was computed according to environment temperature of 300 K and by employing heat transfer coefficient of 5 W/(m²·K). Although large eddy simulation approach to turbulence modelling is already penetrating in the complex industrial applications (Mikulčić et al., 2014), this work employs advanced k- ζ -f turbulence model from the well-established Reynolds Averaged Navier-Stokes (RANS) model group. Compared to the established k- ϵ model, the k- ζ -f turbulence model dispenses with the conventional practice of introducing empirical damping functions. It is more suitable for strong swirling flows such as those that can be found in internal combustion engines. For the turbulence and energy transport equations a first order UPWIND differencing scheme was applied, whilst for the continuity and species transport equations the central differencing scheme (CDS) was employed. The CDS can generate numerical oscillations yielding unbounded and non-monotonic solutions. Therefore, for the momentum equation a combination of CDS and UPWIND was proposed by introducing the blending factor of 0.5 (AVL, 2013). For all calculations the implicit time integration was employed ensuring unconditional solution stability. The solution convergence criterion is achieved when the momentum, pressure, energy and volume fraction residuals decrease under the value of 1e-4. The pressure velocity coupling of the momentum and continuity equation was obtained using the SIMPLE algorithm. Between 0.1 and 0.4 s the mass of 0.4 g of UWS spray with initial velocity of 27 m/s is injected into domain. The droplet disintegration models were replaced by presuming the droplet size distribution. It is of utmost importance to correctly describe the spray process since the evaporation rate and the mixing between the droplet phase and bulk phase directly influence the thermolysis process and NO reduction. The Rosin–Rammler distribution with

exponent of 2.5 was used to represent the non-uniform droplet size distribution since it was shown in previous research (Ström et al., 2009; Varna et al., 2015) to accurately captures droplet size effects of real UWS injection systems. In the following Table, the droplet size distribution was referred to as PSD and also expected droplet diameters are given. It is important to note that still there is no reliable model of droplet interaction with porous catalytic structure, thus during the simulations the option “stop droplet at porosity” was enabled. The interaction of spray droplets with hot catalyst walls was modelled using well established model from Kuhnke (Kuhnke, 2004), which identifies 4 characteristic interaction regimes. The purpose of this work is research of influence of spray injection direction and droplet size on uniformity of ammonia distribution as well as on ammonia slip out of the catalyst. Six different cases were established according to settings depicted in the following Table.

Table 3. Simulation settings –injection direction and droplet size influence

Name	Injection direction	Droplet size
Case_1	 (co-flow)	PSD (160 μm)
Case_2	 (co-flow)	PSD (105 μm)
Case_3	 (co-flow)	PSD (90 μm)
Case_4	 (perpendicular to the main flow)	100 μm
Case_5	 (counterflow)	100 μm
Case_6	 (co-flow)	100 μm

Simulated cases were divided into two groups depicted in the Table 4. according to effects that were thoroughly studied, namely influence of droplet size and injection direction. Following section presents simulation results.

Table 4. Simulation groups

Group 1			Group 2		
Influence of droplet size			Influence of injection direction		
Case_1	Case_3	Case_6	Case_4	Case_5	Case_6

4. RESULTS AND DISCUSSION

First, cases belonging to Group 1 are discussed. Two representative time instances were chosen, namely 0.15 s and 0.4 s. At 0.15 s the spray development through the mixing chamber can be seen, whilst at 0.4 s peak values of NO_x reductants are realized. If we observe distribution of the NH_3 within the SCR system, the fastest propagation is visible in Case_3 at 0.15 s. At 0.4 s a fairly uniform distribution of NH_3 in Case_1 and Case_6 can be observed, while Case_3 has more dispersed NH_3 mass fraction, as depicted in Figure 3. The mass fraction of ammonia is higher in Case_6 and Case_1, which implies they achieve better urea conversion.

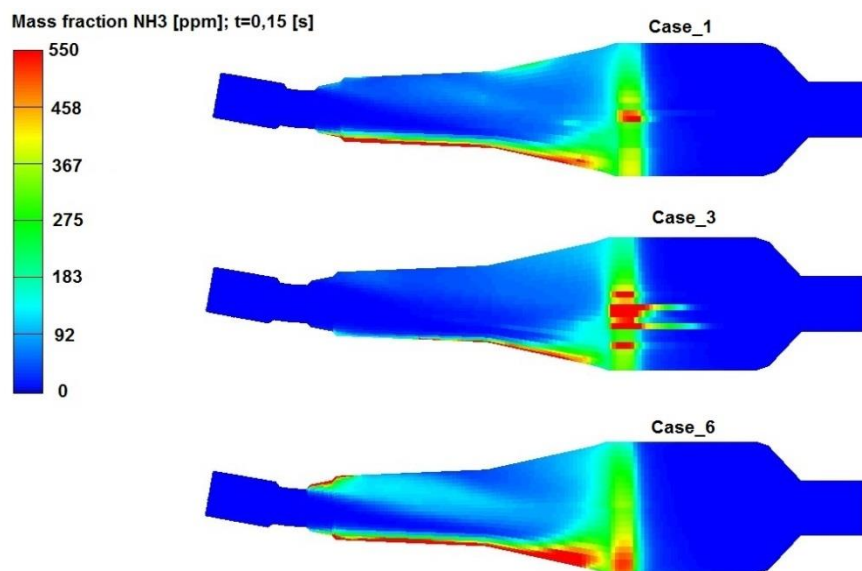


Figure 2. NH_3 mass fraction at 0.15 s

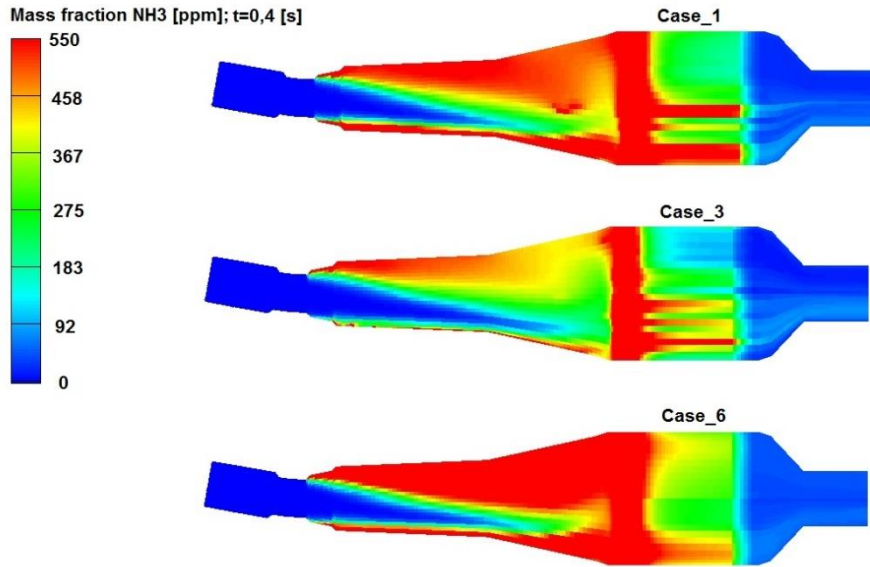


Figure 3. NH_3 mass fraction at 0.4 s

Figure 4. and Figure 5. depict H₂CO mass fraction at the same time instances. From the Figure 4. it can be concluded that the mass fraction and distribution of H₂CO are similar for all of the three observed cases in the early stage of the spray injection. Contrary to that, Figure 5. shows that the highest H₂CO fraction and most homogeneous H₂CO distribution is present in Case_6. Case_1 and Case_3 have less uniform distribution and H₂CO mass fraction is the lowest in Case_3.

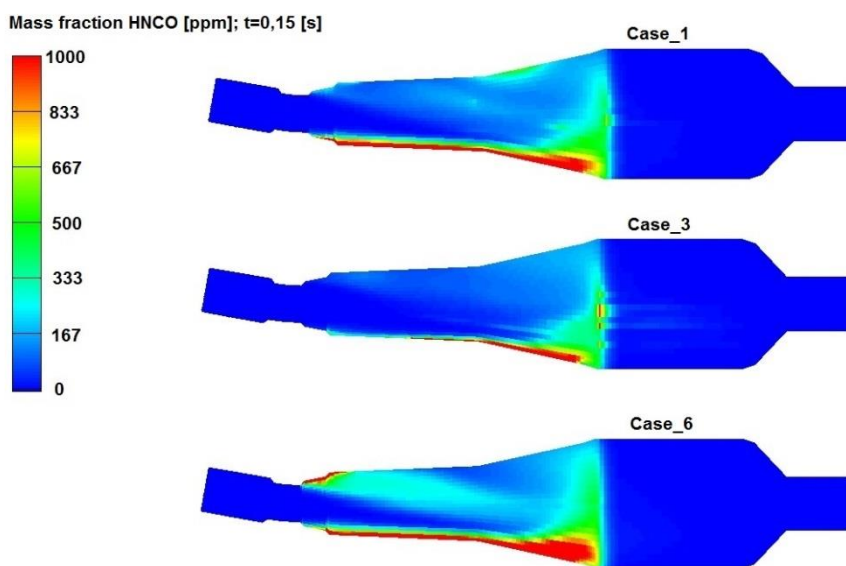


Figure 4. H₂CO mass fraction at 0.15 s

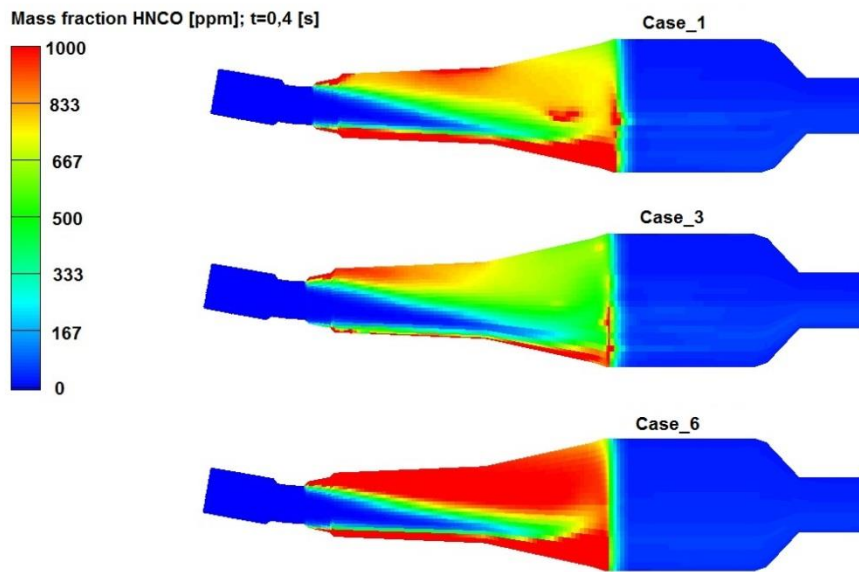


Figure 5. HSCO mass fraction at 0.4 s

NO reduction in Figure 6. is consistent with observations from Figure 2., since the propagation of ammonia is fastest in Case_3, which consequently has strongest initial reduction of NO. Here it should be noted that NO mass fraction drops solely by passing through the catalyst due to the fact that catalyst is loaded with ammonia at the beginning of simulation. Figure 7. shows that all three cases have reduced NO mass fractions on negligible level. This is expected since in all simulated cases the amount of injected urea remains intact. Similar reasoning is also valid for NO₂ which is therefore not depicted.

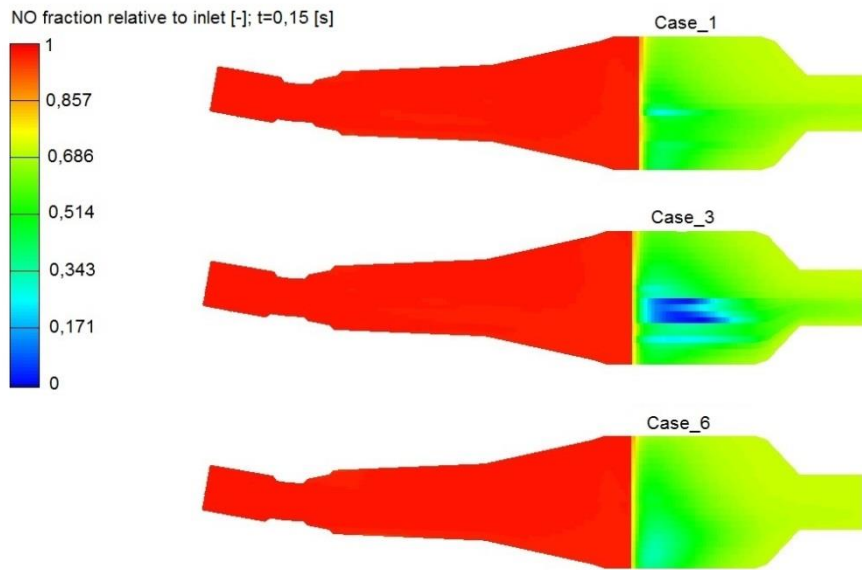


Figure 6. NO conversion at 0.15 s

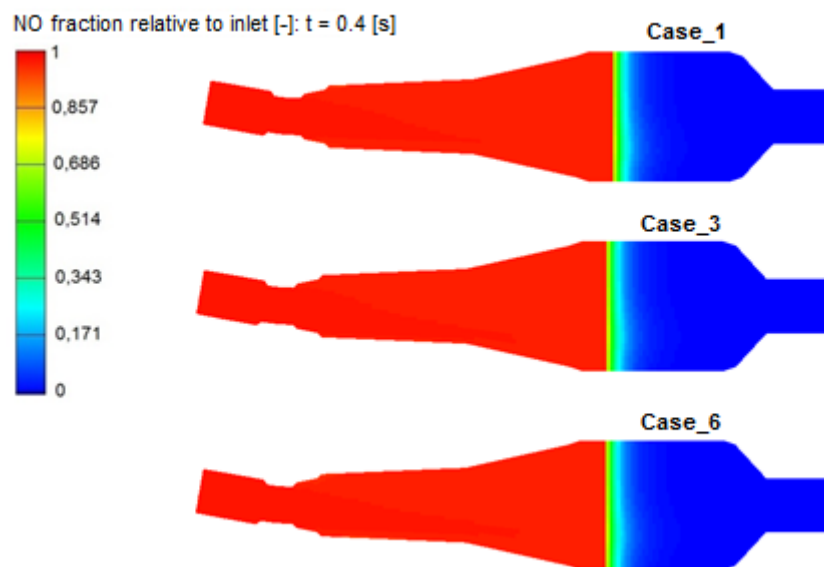


Figure 7. NO conversion at 0.4 s

Water mass fraction of spray droplets can be used as evaporation indicator. It is visible from Figure 8. that Case_6 contains the biggest droplet density. Nevertheless, at the same time the smallest number of droplets impinges on the catalyst surface, indicating the most favourable droplet decomposition. The reason for this behaviour lays in uniform droplet size that, although fairly large, causes droplet to evaporate and decompose more quickly than in Case_1 and Case_3, where droplet stream contains larger droplets that are impinging catalyst surface.

It is also visible that droplets in Case_3 have lower evaporation rate. Case_1 has the highest water mass fraction in the vicinity of nozzle, but the evaporation dynamics is similar to Case_3.

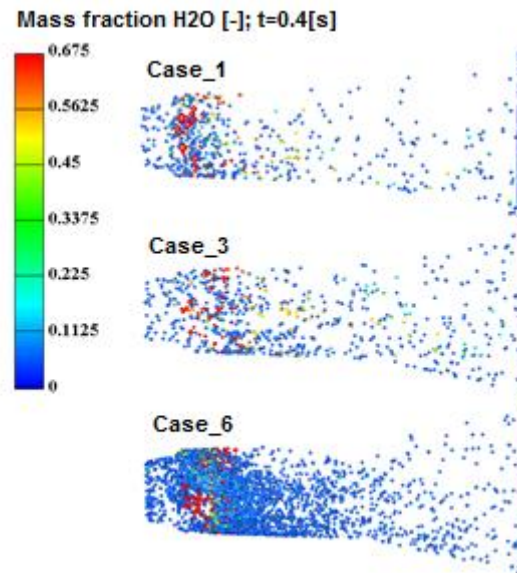


Figure 8. Water fraction in spray droplets at 0.4 s – Group 1

As has been previously stated in Table 4, Group 2 studies the influence of injection direction on the homogenization of ammonia. Figure 9. reveals that spray direction perpendicular to the main flow has the most detrimental effect on the evaporation rate, resulting in a large number of droplets sticking on the catalyst walls. Qualitative observation of Case_5 and Case_6 doesn't reveal significant differences in evaporation dynamics. In order to better study behaviour of two simulation groups, the following section presents analyses of the uniformity of reductant in cross sections bounding the catalyst.

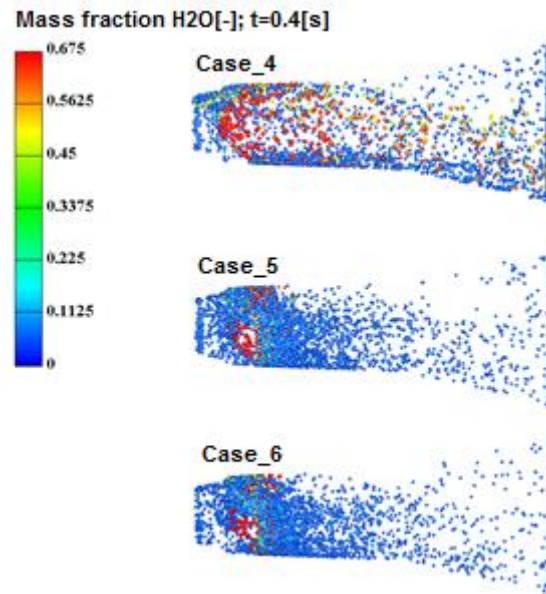


Figure 9. Water fraction in spray droplets at 0.4 s – Group 2

The following analysis has been carried out for the simulation time of 0.4 s since than the maximum of NH₃ concentration is achieved within the system. Thus, it is representative for the evaluation of uniformity of distribution on the catalyst inlet and outlet as one of the key parameters of the SCR process quality.

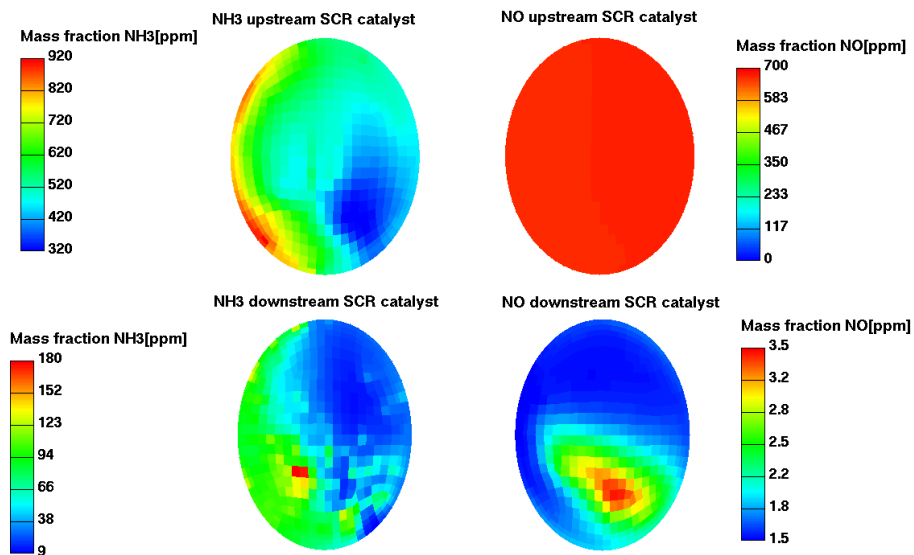


Figure 10. NH₃ and NO mass fraction – Case_1 at 0.4 s

Figure 10. shows fairly uniform distribution of NH_3 on the catalyst inlet with lower right part of cross section deviating from the mean value. After the catalyst exit ammonia mass fractions fall down one order of magnitude indicating favourable ammonia consumption in deNO_x reactions. NO is almost completely reduced at the catalyst exit as only a few ppm of NO slips into environment.

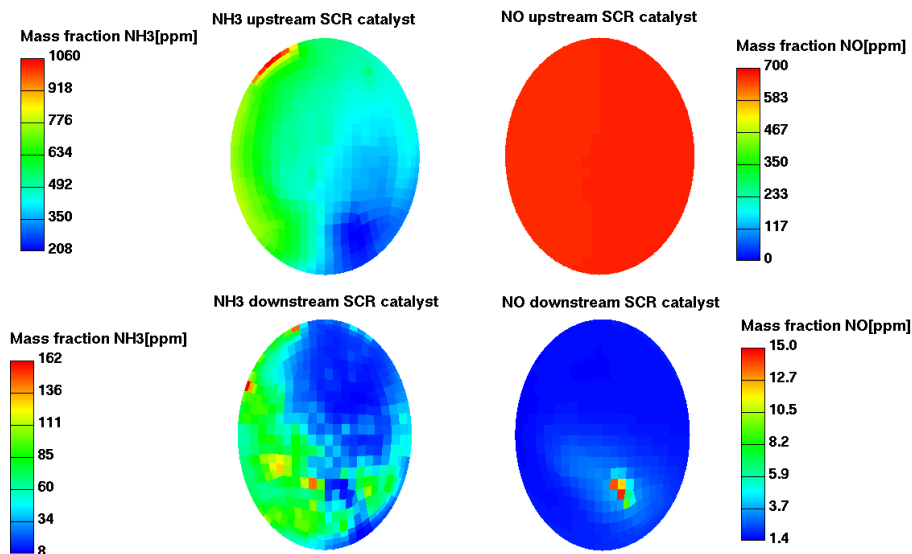


Figure 11. NH_3 and NO mass fraction – Case_2 at 0.4 s

Figure 11. depicts similar ammonia distribution compared to the Case_1 on the catalyst inlet, with higher span of mass fractions. However, more ammonia is consumed during the reactions, so that ammonia slip is lower in this case. There is small area of very low ammonia fraction which is also reflected in the NO distribution on the catalyst exit, where locally higher amount of NO slips to environment. Comparable trend can be observed also on the following Figure 12., which is expected due to similar mean droplet size in Rosin Rammler distribution. This case has the best ammonia uniformity of all the simulated cases, and at this stage is expected that it will have low ammonia slip. Non uniform ammonia distribution may cause uneven catalyst load and consequently deactivation of the catalyst surface due to occurrence of deposits.

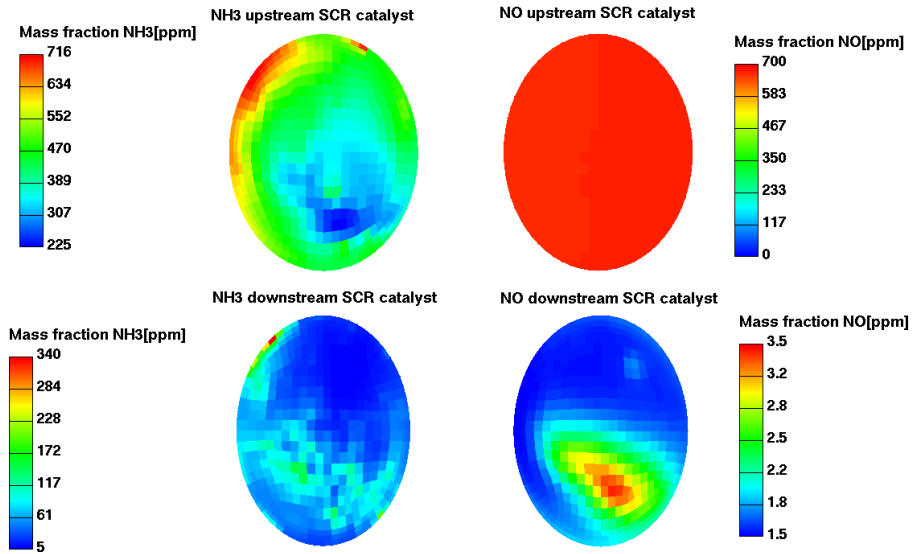


Figure 12. NH₃ and NO mass fraction – Case_3 at 0.4 s

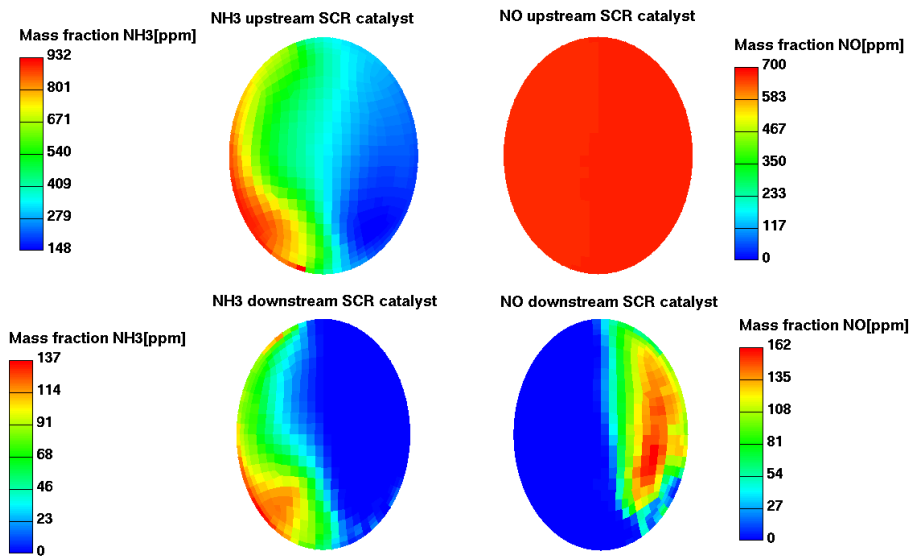


Figure 13. NH₃ and NO mass fraction – Case_4 at 0.4 s

Figure 13. shows strong ammonia non-uniformity on the catalyst inlet as a consequence of perpendicular injection direction. This causes stronger activation of the one half of the catalyst, leading to uneven catalyst aging and with it connected difficulties. Also, it should be noted that this is the only case where NO slip is one order of magnitude higher, exactly on the side where ammonia mass fractions are lower. Case_5 and Case_6 demonstrate somewhat

worse uniformity compared to Case_1, Case_2 and Case_3, but the range of the ammonia slip mass fraction is narrower compared to the same cases. This means that more ammonia is consumed and consequently there will be less ammonia slip, at least on the basis of qualitative observation. In order to quantify all cases following section analyses average species mass fractions along SCR system and finally ammonia slip to environment.

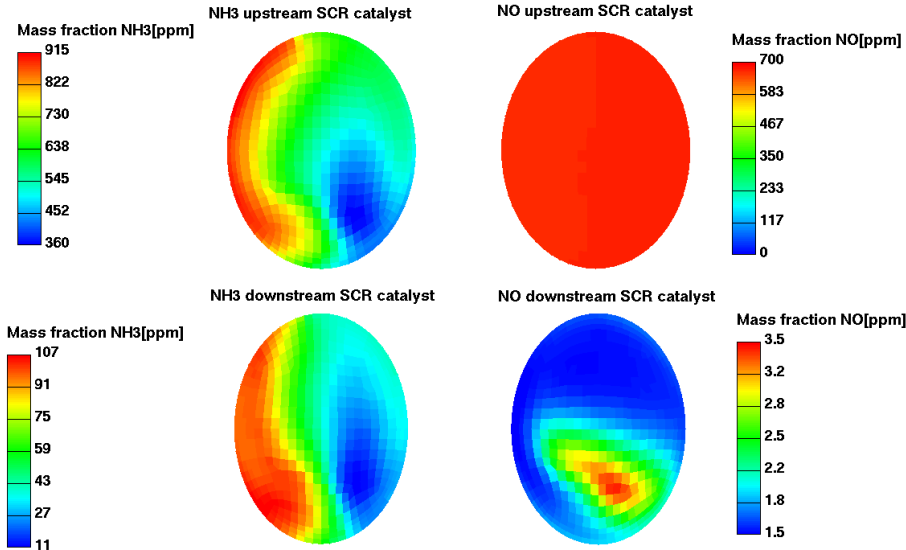


Figure 14. NH₃ and NO mass fraction – Case_5 at 0.4 s

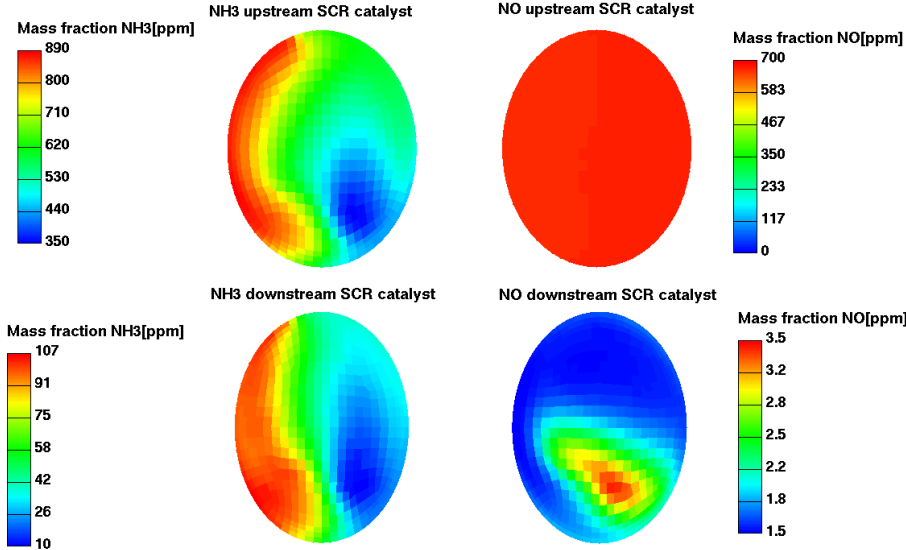


Figure 15. NH₃ and NO mass fraction – Case_6 at 0.4 s

At the beginning of the injection the highest ammonia mass fraction is achieved in the Case_2 which is depicted in the Figure 16. Also, there can be seen slight decrease of mass fraction in Case_2 and Case_3 at 0.7 m due to catalyst geometry, since it facilitates expansion of the geometry on that location, so that generated ammonia can be spread in larger volume. Case_1 doesn't follow observed trend due to larger droplets which evaporate and start to decompose in the expansion of mixing chamber. Here should be also noted that Case_4, Case_5 and Case_6 don't reach the same magnitude of mass fractions, so their value is not depicted. Figure 17. reveals following time step where Case_3 has the highest ammonia mass fraction due to the smallest UWS droplets of all simulated cases. The rest of simulated cases show similar ammonia mass fraction along SCR system with previously explained Case_4 as an exception.

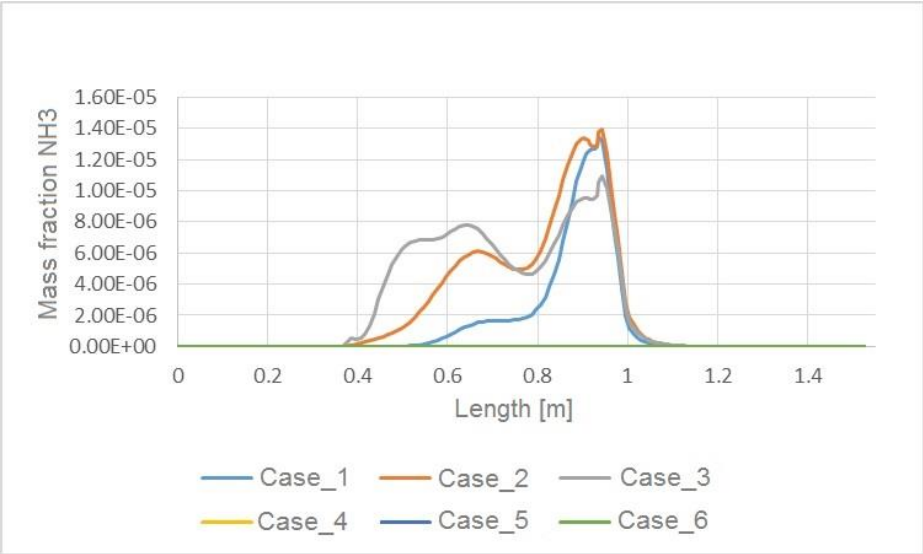


Figure 16. NH₃ mass fraction along SCR system at 0.11 s

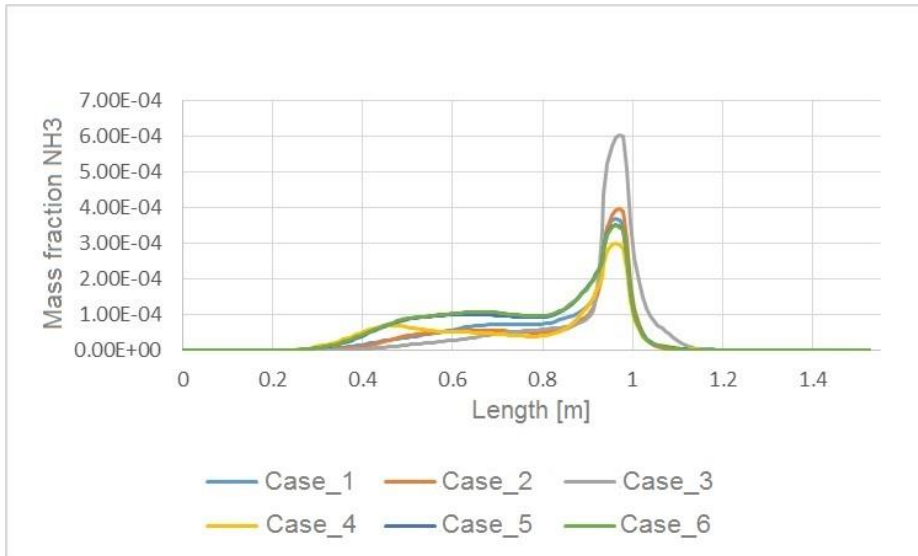


Figure 17. NH₃ mass fraction along SCR system at 0.15 s

The time instance 0.4 s after the beginning of simulation was chosen due to the fact that then the highest reductant fraction is achieved before the catalyst inlet. It can be seen in Figure 18. that the highest ammonia mass fraction was achieved for the Case_1 followed by Case_2, Case_6, Case_5 and finally, Case_3 and Case_4 with the lowest mass fraction. Counterflow injection is by no means worse than co-flow injection. Sudden peak of ammonia for all cases depicted in the Figure 18. is the consequence of hydrolysis of isocyanic acid in the catalyst during which the additional ammonia is generated.

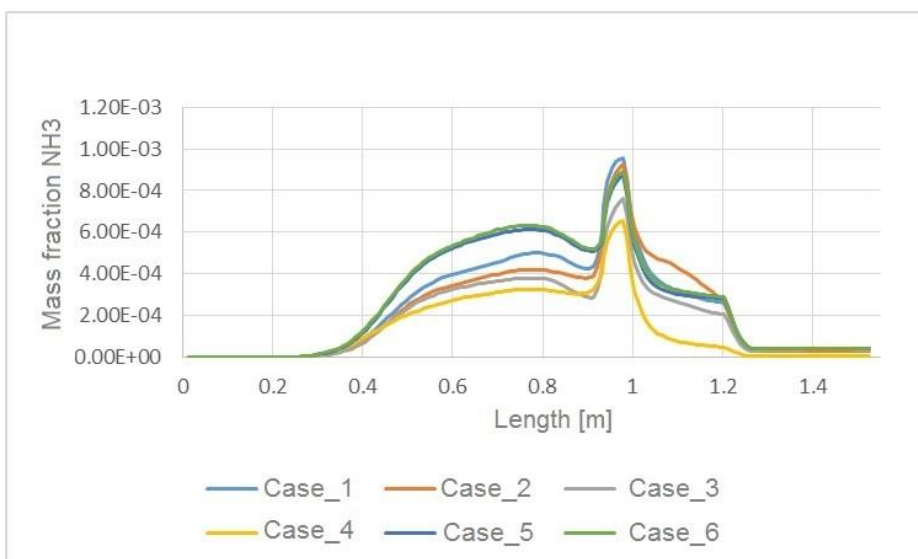


Figure 18. NH₃ mass fraction along SCR system at 0.4 s

Figure 19. shows isocyanic acid results after 0.4 s where similar trends as in ammonia case can be observed. The sudden drop in mass fraction is attributed to the beginning of the catalyst where hydrolysis of HNCO is taking place. Finally, this section can be concluded by the fact that larger droplets achieve higher ammonia and isocyanic acid mass fractions at the catalyst inlet, but one should bear in mind that larger droplets also result in more intense impingement on catalyst wall, which can, depending on local flow conditions, lead to difficulties associated with deposit formation.

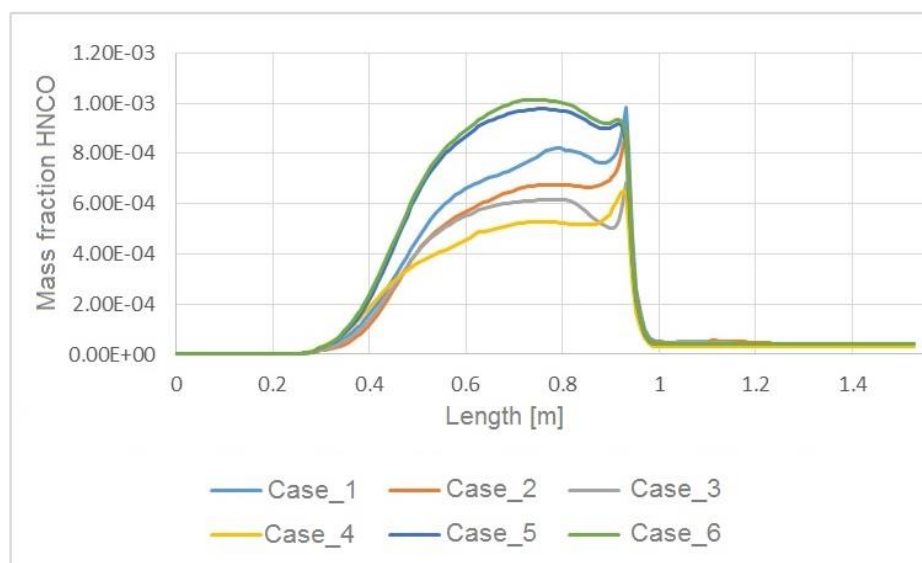


Figure 19. HNCO mass fraction along SCR system at 0.4 s

Figure 20. shows ammonia slip from the catalyst as important design parameter due to its toxicity and harmful environmental impact. All of the simulated cases have similar ammonia slip, except Case_5 which has a reduction of around 40 % compared to other cases. Regardless the fact that Case_3 has the most uniform ammonia distribution, counterflow direction provided longer residence time of ammonia, enabling thus greater consumption of ammonia and therefore lowest ammonia slip. Exhaust gas stream should first decelerate droplets and change their direction, then accelerate them again, which finally has beneficial impact on the generation of ammonia and reaction progress before the catalyst.

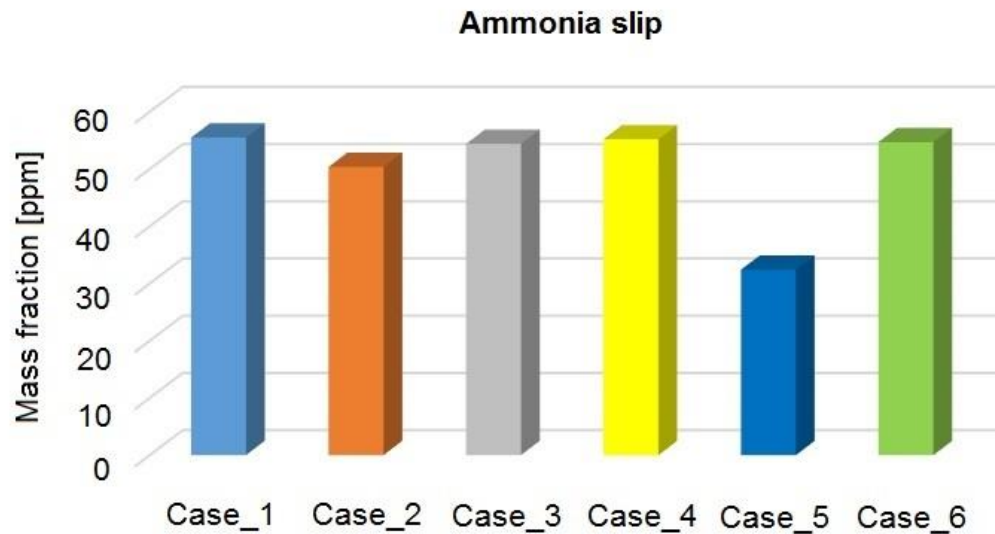


Figure 20. Comparison of ammonia slip for simulated cases

5. CONCLUSION

This paper presented CFD modelling capabilities of physical phenomena taking place in the SCR process, from the urea injection, to the catalyst monolith exit. After the literature review, relevant mathematical models composing numerical framework for UWS-SCR were described. Afterwards, a 3D turbulent reacting flow CFD model involving reaction mechanism on the catalyst surface was applied on the real SCR system geometry with exhaust gas composition, flow rate and temperature resembling those of diesel engines. Six simulated cases were divided into two simulation groups in order to study the influence of injection direction and droplet size on ammonia generation and uniformity. It has been shown that the best result in terms of ammonia uniformity gives Case_3. Case_4, where UWS was injected perpendicularly to the main flow, was the worst one in terms of ammonia uniformity and NO_x reduction, since this was the only case where one order of magnitude higher mass fraction of NO_x slipped in the environment. Although injection direction didn't provide better ammonia uniformity, it has strong impact on minimization of ammonia slip to environment due to longer residence time of

droplets and ammonia in the system in the case of counterflow injection. This finding indicates that ammonia uniformity before the catalyst is not the only indicator of SCR process quality, but also residence time of the reagent should be taken into account. Counterflow injection of UWS achieved minimum ammonia slip, 40 % lower than in other cases. This becomes more important in the light of the fact that ammonia slip is also regulated by EURO 6 standard for heavy duty diesel vehicles. Despite the fact that counterflow injection is still in the research phase, it should be taken into account in the further research, especially regarding deposit formation and injector device clogging. From numerical point of view, there is still lack of suitable droplet/porosity interaction model which should be subjected to future work.

ACKNOWLEDGMENTS

Financial support for conducting this research, as well as software support from the AVL List GmbH is gratefully acknowledged.

REFERENCES

- Abramzon, B., Sirignano, W.A., 1989. Droplet vaporization model for spray combustion calculations. *Int. J. Heat Mass Transf.* 32, 1605–1618. doi:10.1016/0017-9310(89)90043-4
- Abu-Ramadan, E., Saha, K., Li, X., 2011. Modeling the depleting mechanism of urea-water-solution droplet for automotive selective catalytic reduction systems. *AIChE J.* 57, 3210–3225. doi:10.1002/aic.12523
- AVL, 2013. FIRE ® VERSION 2013.2 manual.
- Baleta, J., 2013. Numerical investigation of wallfilm formation for selective catalytic reduction applications. University of Zagreb.
- Baleta, J., Mikulčić, H., Vujanović, M., Petranović, Z., Duić, N., 2016. Numerical simulation

of urea based selective non-catalytic reduction deNO_x process for industrial applications.
Energy Convers. Manag. doi:10.1016/j.enconman.2016.01.062

Betageri, V., Rajagopalan, M., Dhakshina Murthy, S., Thondavadi, A., 2016. Effects of Diesel Exhaust Fluid (DEF) Injection Configurations on Deposit Formation in the SCR System of a Diesel Engine. doi:10.4271/2016-28-0109

Birkhold, F., Meingast, U., Wassermann, P., Deutschmann, O., 2007. Modeling and simulation of the injection of urea-water-solution for automotive SCR DeNO_x-systems. Appl. Catal. B Environ. 70, 119–127. doi:10.1016/j.apcatb.2005.12.035

Cause of climate change [WWW Document], n.d. URL http://ec.europa.eu/clima/change/causes/index_en.htm (accessed 7.28.15).

Chen, Y., Lv, L., 2015. Design and evaluation of an Integrated SCR and exhaust Muffler from marine diesels. J. Mar. Sci. Technol. 20, 505–519. doi:10.1007/s00773-014-0302-1

Cho, Y.S., Lee, S.W., Choi, W.C., Yoon, Y.B., 2014. Urea-SCR system optimization with various combinations of mixer types and decomposition pipe lengths. Int. J. Automot. Technol. 15, 723–731. doi:10.1007/s12239-014-0075-x

Choi, C., Sung, Y., Choi, G.M., Kim, D.J., 2015. Numerical analysis of NO_x reduction for compact design in marine urea-SCR system. Int. J. Nav. Archit. Ocean Eng. 7, 1020–1034. doi:10.1515/ijnaoe-2015-0071

Dukowicz, J.K., 1979. Quasi-steady droplet phase change in the presence of convection.

EEA, 2014. Emissions of the main air pollutants in Europe [WWW Document]. URL <http://www.eea.europa.eu/data-and-maps/indicators/main-anthropogenic-air-pollutant-emissions/assessment-3> (accessed 12.30.16).

European Environment Agency, n.d. Nitrogen oxides (NO_x) emissions [WWW Document].

URL <http://www.eea.europa.eu/data-and-maps/indicators/eea-32-nitrogen-oxides-nox-emissions-1/assessment.2010-08-19.0140149032-3> (accessed 7.15.15).

European Union, Regulation (EC) No 715/2007, 2007.

Fang, H.L., DaCosta, H.F.M., 2003. Urea thermolysis and NO_x reduction with and without SCR catalysts. *Appl. Catal. B Environ.* 46, 17–34. doi:10.1016/S0926-3373(03)00177-2

Grout, S., Blaisot, J.-B., Pajot, K., Osbat, G., 2013. Experimental investigation on the injection of an urea–water solution in hot air stream for the SCR application: Evaporation and spray/wall interaction. *Fuel* 106, 166–177. doi:10.1016/j.fuel.2012.09.022

Hanjalić, K., Popovac, M., Hadžiabdić, M., 2004. A robust near-wall elliptic-relaxation eddy-viscosity turbulence model for CFD. *Int. J. Heat Fluid Flow* 25, 1047–1051. doi:10.1016/j.ijheatfluidflow.2004.07.005

Honus, S., Kumagai, S., Němček, O., Yoshioka, T., 2016. Replacing conventional fuels in USA, Europe, and UK with plastic pyrolysis gases – Part I: Experiments and graphical interchangeability methods. *Energy Convers. Manag.* 126, 1118–1127. doi:10.1016/j.enconman.2016.08.055

Jeong, S.-J., Lee, S.-J., Kim, W.-S., 2008. Numerical Study on the Optimum Injection of Urea–Water Solution for SCR DeNO_x System of a Heavy-Duty Diesel Engine to Improve DeNO_x Performance and Reduce NH₃ Slip. *Environ. Eng. Sci.* 25, 1017–1036. doi:10.1089/ees.2007.0224

Kozarac, D., Vuilleumier, D., Saxena, S., Dibble, R.W., 2014. Analysis of benefits of using

- internal exhaust gas recirculation in biogas-fueled HCCI engines. *Energy Convers. Manag.* 87, 1186–1194. doi:10.1016/j.enconman.2014.04.085
- Kuhnke, D., 2004. Spray Wall Interaction Modelling by Dimensionless Data Analysis. PhD thesis. TU Darmstadt.
- Lee, J.-G., Kim, Y.-D., Kim, W.-S., 2012. Design and Implementation of Mixing Chambers to Improve Thermal Decomposition of Urea for NO X Abatement. *Environ. Eng. Sci.* 29, 979–986. doi:10.1089/ees.2011.0414
- Liao, Y., Dimopoulos Eggenschwiler, P., Spiteri, A., Nocivelli, L., Montenegro, G., Boulouchos, K., 2015. Fluid Dynamic Comparison of AdBlue Injectors for SCR Applications. *SAE Int. J. Engines* 8, 2015-24–2502. doi:10.4271/2015-24-2502
- Mikulčić, H., von Berg, E., Vujanović, M., Wang, X., Tan, H., Duić, N., 2016. Numerical evaluation of different pulverized coal and solid recovered fuel co-firing modes inside a large-scale cement calciner. *Appl. Energy*. doi:10.1016/j.apenergy.2016.05.012
- Mikulčić, H., Vujanović, M., Ashhab, M.S., Duić, N., 2014. Large eddy simulation of a two-phase reacting swirl flow inside a cement cyclone. *Energy* 75, 89–96. doi:10.1016/j.energy.2014.04.064
- Mujeebu, M.A., Abdullah, M.Z., Bakar, M.Z.A., Mohamad, A.A., Muhad, R.M.N., Abdullah, M.K., 2009. Combustion in porous media and its applications – A comprehensive survey. *J. Environ. Manage.* 90, 2287–2312. doi:10.1016/j.jenvman.2008.10.009
- Musa, S. N. A., Saito, M., Furuhashi, T., Arai, M., 2006. Evaporation Characteristics of a Single Aqueous Urea Solution Droplet, in: ICLASS 2006.
- Oh, J., Lee, K., 2014. Spray characteristics of a urea solution injector and optimal mixer

location to improve droplet uniformity and NO_x conversion efficiency for selective catalytic reduction. *Fuel* 119, 90–97. doi:10.1016/j.fuel.2013.11.032

Petranović, Z., Edelbauer, W., Vujanović, M., Duić, N., 2017. Modelling of spray and combustion processes by using the Eulerian multiphase approach and detailed chemical kinetics. *Fuel* 191, 25–35. doi:10.1016/j.fuel.2016.11.051

S. Kontin, A. Höfler, R. Koch, H.-J.B., 2010. Heat and Mass Transfer accompanied by Crystallisation of single Particles containing Urea-water-solution, in: *Proceedings of 23rd ILASS-2010*. ILASS, Brno.

Sadashiva Prabhu, S., Nayak, N.S., Kapilan, N., Hindasageri, V., 2017. An experimental and numerical study on effects of exhaust gas temperature and flow rate on deposit formation in Urea-Selective Catalytic Reduction (SCR) system of modern automobiles. *Appl. Therm. Eng.* 111, 1211–1231. doi:10.1016/j.applthermaleng.2016.09.134

Smith, H., Lauer, T., Mayer, M., Pierson, S., 2014. Optical and Numerical Investigations on the Mechanisms of Deposit Formation in SCR Systems. *SAE Int. J. Fuels Lubr.* 7, 2014-01–1563. doi:10.4271/2014-01-1563

Ström, H., Lundström, A., Andersson, B., 2009. Choice of urea-spray models in CFD simulations of urea-SCR systems. *Chem. Eng. J.* 150, 69–82. doi:10.1016/j.cej.2008.12.003

Tayyeb Javed, M., Irfan, N., Gibbs, B.M., 2007. Control of combustion-generated nitrogen oxides by selective non-catalytic reduction. *J. Environ. Manage.* 83, 251–289. doi:10.1016/j.jenvman.2006.03.006

Tian, X., Xiao, Y., Zhou, P., Zhang, W., 2015. Optimization of the location of injector in

urea-selective catalytic reduction system. *J. Mar. Sci. Technol.* 20, 238–248.
doi:10.1007/s00773-014-0267-0

Varna, A., Spiteri, A.C., Wright, Y.M., Dimopoulos Eggenschwiler, P., Boulouchos, K., 2015. Experimental and numerical assessment of impingement and mixing of urea–water sprays for nitric oxide reduction in diesel exhaust. *Appl. Energy* 157, 824–837.
doi:10.1016/j.apenergy.2015.03.015

Wang, T.J., Baek, S.W., Lee, S.Y., Kang, D.H., Yeo, G.K., 2009. Experimental investigation on evaporation of urea-water-solution droplet for SCR applications. *AIChE J.* 55, 3267–3276. doi:10.1002/aic.11939

Winkler, C., Flörchinger, P., Patil, M.D., Gieshoff, J., Spurk, P., Pfeifer, M., 2003. Modeling of SCR DeNO_x Catalyst - Looking at the Impact of Substrate Attributes.
doi:10.4271/2003-01-0845

Wurzenberger, J.C., Wanker, R., 2005. Multi-Scale SCR Modeling, 1D Kinetic Analysis and 3D System Simulation. doi:10.4271/2005-01-0948

Yim, S.D., Kim, S.J., Baik, J.H., Nam, I.S., Mok, Y.S., Lee, J.H., Cho, B.K., Oh, S.H., 2004. Decomposition of urea into NH₃ for the SCR process. *Ind. Eng. Chem. Res.* 43, 4856–4863. doi:10.1021/ie034052j

Yuen, M.C., Chen, L.W., 1976. On Drag of Evaporating Liquid Droplets. *Combust. Sci. Technol.* 14, 147–154. doi:10.1080/00102207608547524

Zhang, H., Wang, J., 2016. Adaptive Sliding-Mode Observer Design for a Selective Catalytic Reduction System of Ground-Vehicle Diesel Engines. *IEEE/ASME Trans. Mechatronics* 21, 2027–2038. doi:10.1109/TMECH.2016.2542362

Zhang, H., Wang, J., Wang, Y.-Y., 2016. Optimal Dosing and Sizing Optimization for a Ground-Vehicle Diesel-Engine Two-Cell Selective Catalytic Reduction System. *IEEE Trans. Veh. Technol.* 65, 4740–4751. doi:10.1109/TVT.2015.2476760

Figure captions:

Figure 1. Discretized geometry of the SCR system

Figure 2. NH_3 mass fraction at 0.15 s

Figure 3. NH_3 mass fraction at 0.4 s

Figure 4. HNCO mass fraction at 0.15 s

Figure 5. HNCO mass fraction at 0.4 s

Figure 6. NO conversion at 0.15 s

Figure 7. NO conversion at 0.4 s

Figure 8. Water fraction in spray droplets at 0.4 s – Group 1

Figure 9. Water fraction in spray droplets at 0.4 s – Group 2

Figure 10. NH_3 and NO mass fraction – Case_1 at 0.4 s

Figure 11. NH_3 and NO mass fraction – Case_2 at 0.4 s

Figure 12. NH_3 and NO mass fraction – Case_3 at 0.4 s

Figure 13. NH_3 and NO mass fraction – Case_4 at 0.4 s

Figure 14. NH_3 and NO mass fraction – Case_5 at 0.4 s

Figure 15. NH_3 and NO mass fraction – Case_6 at 0.4 s

Figure 16. NH_3 mass fraction along SCR system at 0.11 s

Figure 17. NH_3 mass fraction along SCR system at 0.15 s

Figure 18. NH_3 mass fraction along SCR system at 0.4 s

Figure 19. HNCO mass fraction along SCR system at 0.4 s

Figure 20. Comparison of ammonia slip for simulated cases

Table captions:

Table 1. Variation of time step size for simulation

Table 2. Exhaust gas composition on the inlet

Table 3. Simulation settings –injection direction and droplet size influence

Table 4. Simulation groups